Journal of Analytical and Applied Pyrolysis 159 (2021) 105322

Contents lists available at ScienceDirect

Journal of Analytical and Applied Pyrolysis

journal homepage: www.elsevier.com/locate/jaap

Upcycling simulated food wastes into superactivated hydrochar for remarkable hydrogen storage

Al Ibtida Sultana, Nepu Saha, M. Toufiq Reza *

Department of Biomedical and Chemical Engineering and Sciences, Florida Institute of Technology, 150 West University Boulevard, Melbourne, FL 32901, USA

ARTICLE INFO

Keywords:
Food waste
Hydrothermal carbonization
Chemical activation
Super activated hydrochar
Hydrogen storage

ABSTRACT

In an effort of developing hydrogen storage material, the goal of this study was to explore the potential of the abounding food waste biomass as a precursor for the development of porous carbon materials for remarkable hydrogen storage. Therefore, in this study, simulated food waste, a mixture of six commonly disposed food items (apple, bread, green bean, cabbage, cheese, and canned chicken), was hydrothermally carbonized at 220 °C followed by chemical activation at 800 °C using various activating agent (KOH) to food waste hydrochar ratio (i.e., 2:1, 3:1 and 4:1). The solid products, hereafter called superactivated hydrochars, were characterized by proximate and ultimate analyses as well as X-ray diffractometer (XRD) and through nitrogen adsorption isotherms at 77 K to analyze the changes in the material including its surface porosity parameters (surface area, pore volume, and pore size distribution) as the food waste underwent chemical and morphological modifications. The gravimetric (wt%) hydrogen storage capacity of the superactivated hydrochars were then conducted under 77 K and various pressure of 0–23 bar. Results showed that the surface area and total pore volume in the superactivated hydrochars were in the range of, as high as, 2070 to 2885 m^2/g and 0.98 to 1.93 cm^3/g, respectively. The remarkable hydrogen storage capacity was observed of as high as 6.15 wt% at 23 bar and 77 K for the superactivated hydrochar produced with a KOH to food waste hydrochar ratio of 4:1. This distinctly highlights the pertinent upcycling technique of food waste to be effective in developing efficient hydrogen storage material.

1. Introduction

While hydrogen (H_2) and energy have a long shared history from 200 years ago in powering the first internal combustion engines, for the past two decades there has been an escalating momentum of interest in hydrogen as it is a zero-emission energy and hence an answer to the growing concern over increasing carbon emission and energy security for a prospective clean and secure energy economy [1–3]. With its favorable characteristics as an energy carrier (non-toxic, sustainable and the lightest element with the highest energy content of 142 MJ/kg of higher heating value) [4–8], the escalating demand of hydrogen in the U.S. can be projected to reach 63 million tons by 2050 which will share about 14 % of the total energy demand [9]. While significant progress has been made in producing hydrogen either from natural gas, coal, water, or biomass [10–19], development of high-performance, low-cost and environmentally-friendly hydrogen storage medium is one of the substantial challenges where the key to the solution is design of novel material and utilization of synthesis processes that allow a precise control over the structural characteristics (e.g. surface porosity) of the developed material [20].

Recently, biomass-derived porous carbon materials have engaged considerable interest in the emergent application of hydrogen storage because of their abundance and low cost, superior chemical, mechanical, and thermal stability as well as ease of regeneration and configurable pore structure [6,21]. From recent literature, such porous carbons were developed with the ability of storing hydrogen as high as 8.9 wt% and 1.2 wt% at 77 K and 295 K, respectively, at 30 bar, owing to the combination of high surface porosity as well as favorable surface functionality [7]. However, in quest of suitable porous carbon for hydrogen storage, globally abundant biomass of food waste (FW) would seem highly desirable to be employed as an inexpensive, sustainable, and novel next-generation precursor in preparing hydrogen gas adsorbent. The purpose can be further explained with words of Prof. Donald Sadoway from The Missing Link to Renewable Energy: *"(…) if you want to make something dirt cheap, make it out of dirt … and preferably dirt that's locally sourced*" [22]. FW is generally defined as the organic waste that is

* Corresponding author.
E-mail address: treza@fit.edu (M.T. Reza).

https://doi.org/10.1016/j.jaap.2021.105322
Received 24 March 2021; Received in revised form 7 August 2021; Accepted 2 September 2021
Available online 4 September 2021

discharged from various sources, comprising of food processing plants, domestic and commercial kitchens, cafeterias and restaurants [23]. Whereas the global volume of FW is estimated as 1.6 billion tons annually, it is projected to boom to a level of 2.1 billion tons by 2030 [24,25]. According to U.S. Environmental Protection Agency (EPA), U.S. is one of the global leaders in FW, where almost 40 million tons of food is discarded every year and this is forecast to reach approximately 66 million tons by 2030 [26,27]. It is therefore admonished to find avenues of upcycling FW into higher value materials such as hydrogen storage medium.

One of the challenges to upcycle FW is the high moisture content (typically 70 % by mass) [28–30], which makes most thermochemical conversion processes not viable, except for hydrothermal carbonization (HTC), which is energetically more favorable by being advantageous for wet-biomass (moisture content of 80–90 %) conversion [31,32]. HTC treatment generally uses the residual moisture of the feedstock as the reaction medium and usually conducted between 180−260 °C with pressure above the water's saturation pressure for a duration of 5 min up to 8 h [33,34]. HTC is therefore an environmentally-friendly pathway for generating carbon-dense homogeneous solid product (hydrochar) with excess oxygen containing functional groups from wet heterogeneous organic feedstocks like FW [35–37]. Owing to such suitable chemical characteristics of hydrochar (carbon-dense, surface functionality and low degree of aromatization), several authors pioneered subjecting hydrochar to additional heat treatment for the development of porous activated carbons for hydrogen storage via controlled chemical activation as hydrochar has the drawback of possessing very low porosity [38–41]. However, chemical activation of hydrochar could significantly increase the porosity and surface area of hydrochar [41–45]. Traditionally, chemical activation utilizes KOH, NaOH, H_3PO_4 or $ZnCl_2$ at a temperature in the 450–900 °C range [46]. Literature encourages KOH as activating agent as it results in the development of ultra-large surface area (1500–3800 m^2/g) from a variety of precursors (coal, polymers, biomass or hydrochar, graphene, etc.) [7,20,47]. In addition to surface porosity, although surface functionality is also a considerable factor of hydrogen uptake capacity, the adsorption capacity is primarily driven by surface area and pore structure as small pore size greatly enhance the fundamental property of interaction energy between hydrogen and the adsorbent [48]. As such, the surface porosity is essentially tailored by means of varying activating conditions where activation ratio, compared to activation temperature, has more influence in terms of porosity development to facilitate hydrogen storage [49–52]. It has been previously demonstrated that the suitable activation temperature for porosity development was in the range of 750−800 °C, due to higher reactivity of hydrochar at higher temperature as well as the generation of H_2O and CO_2 during activation that enhanced pore evolution by simultaneously promoting physical activation [50,53,54]. However, with the variation in the biomass precursor utilized in different studies, the favorable activation ratio showed discrepancy, thus requiring individual investigation of activation ratio to analyze its effect on surface porosity development and hence hydrogen storage capacity [50,53,55–57].

In this study, FW was employed to be developed into a novel and inexpensive hydrogen storage material which to the best of authors' knowledge was first to be reported. HTC of the FW was conducted at 220 °C following by the activation at 800 °C in presence of KOH with various ratio of FW derived hydrochar to KOH (2:1, 3:1 and 4:1) such that the surface porosity was configured in the goal of developing hydrogen storage material with remarkable adsorption capacity. The surface properties of the FW, FW-derived hydrochar, and superactivated hydrochar were characterized in terms of surface area, pore volume, pore size, and crystallinity. Finally, the hydrogen gas storage capacity of the material was studied under cryogenic nitrogen temperature (77 K) at various pressure up to 23 bar.

2. Materials and methodology

2.1. Materials

The feedstock used in this study was a mixture representative of FW that included six commonly disposed food items. These items were mutually selected based on simulated food waste components previously used in various literature [58–60]. All the ingredients were purchased from a local grocery shop at Melbourne, FL and packaging were removed prior to chopping. All the food waste components were chopped and randomly mixed in a food processor as done previously in various literature [60,61]. Solid ingredients as well as the percentage and moisture content of each ingredient are listed in Table 1.Although moisture content of individual ingredient varied between 37 − 94 %, the overall average moisture content of the mixed food waste was 70.5 %. To activate the FW hydrochar, anhydrous potassium hydroxide (KOH) pellets was used as the activating agent which was purchased from Fisher Scientific (Fair Lawn, NJ).

2.2. Material synthesis

HTC of FW was carried out in a 300 mL Parr reactor (Moline, IL) for 30 min at 220 °C. As no significant changes in the ultimate and proximate analyses were found for the hydrochar produced from FW at higher HTC temperature (> 220 °C) [62], the treatment temperature of this study was chosen to be 220 °C. Moreover, it was found in literature that hydrochars produced from higher HTC temperature than 220 °C resulted in a more ordered microstructure and lower amount of oxygen groups, which are more difficult to activate [50,63]. Consequently, it was asserted that lower carbonization temperatures generally assist in porosity development on subsequent activation.

For a typical HTC, the reactor was loaded with 1:10 dry mass of FW to deionized (DI) water ratio. The reactor was sealed, and the content was stirred at 150 ± 5 rpm until the end of the HTC process. Reactor temperature was controlled using a proportional-integral-differentiate (PID) controller while the heating rate was maintained at 10 °C/min. When the reactor temperature reached to the desired HTC temperature of 220 °C, the temperature was kept isothermal for 30 min. The pressure was not controlled but monitored throughout the HTC treatment, which was about 650 ± 20 psi at the highest reaction temperature (220 °C). At the end of the HTC reaction time, the heater was turned off and the reactor was quenched by an ice water bath. It took 15 ± 5 min to cool down the reactor below 50 °C. Produced gases were vented in the fume hood and the process liquid was separated from the solid hydorchar using Whatman 41 filter paper via a vacuum filtration system. The hydrochar was first washed with approx. 200 mL DI water to remove the HTC liquid products adhered to the hydrochar and then dried at 105 °C for 24 h in an oven and stored in a centrifuge tube for further uses. Dried samples were labeled as FW−HC, where HC stands for hydrochar.

The dried hydrochar was then activated using KOH at three different KOH /hydrochar (wt/wt) ratios, such as 2:1, 3:1 and 4:1. The required proportional amount of KOH was ground using mortar-pestle before physically mixing with the hydrochar. Each mixture of KOH and

Table 1
List of food ingredients with their composition and moisture contents used in the simulated food waste feedstock.

Food Item	Percentage composition (dry mass basis)	Moisture content (%)
Apple	6.7 ± 0.5	89.5 ± 0.5
Bread	58.2 ± 0.9	37.2 ± 0.9
Green Bean	4.6 ± 0.4	92.6 ± 0.4
Cabbage	2.6 ± 0.1	94.1 ± 0.1
Cheese	21.4 ± 0.1	61.8 ± 0.1
Canned Chicken	6.5 ± 0.9	73.6 ± 0.9

hydrochar was placed in an alumina crucible and placed in a horizontal MTI series tube furnace (OTF-1200X-S-HPCVD) (Richmond, CA). The mixture was heated at 800 °C for 2 h under a nitrogen flow of 1 L/min. After activation, the samples were washed with 2 N HCl to remove the inorganic impurities and then washed with excessive deionized water until neutral pH was obtained. It was then dried in an oven at 105 °C for 24 h. Dried superactivated hydrochars were labeled as FW-SAH-R, where SAH stands for superactivated hydrochar, R is for the ratio of KOH/hydrochar. The dried samples were stored in centrifuge tubes for further analysis.

2.3. Material characterization

Elemental analysis of samples was carried out with a FLASH EA 1112 Series elemental analyzer (Thermo Scientific, Grand Island, NY) to determine carbon, hydrogen, nitrogen and sulfur contents (wt%). For the analysis, 5-tert-butyl-benzoxazol-2-yl thiophene (BBOT) was used as a calibration standard and vanadium oxide (V_2O_5) as a conditioner for the samples, which were combusted around 950 °C in ultra-high purity oxygen with helium carrier gas and passed over copper oxide pellets and then electrolytic copper. The gases were then analyzed by a thermal conductivity detector (TCD), with the peak areas of detection being compared to that of BBOT standards. The oxygen content was found by the method of difference [64].

Proximate analysis was conducted to determine volatile matter, fixed carbon, and ash content of samples by thermogravimetric analyzer (TGA) using a TGA Q500 (TA instruments, New Castle, DE). A nitrogen atmosphere was used for proximate analysis. Nitrogen gas flowrate and sample heating rates were set at 40 mL/min and 20 °C/min, respectively. Samples were heated from 25 °C to 105 °C and held at 105 °C for 5 min. Temperature was then increased to 850 °C and then held for 5 min. Air was then introduced for 10 min to combust the remaining sample left at 850 °C. The mass loss under the nitrogen atmosphere at 105 °C was considered as moisture whereas mass loss between 105 °C and 850 °C was considered volatile matter. The solid residue at the end of combustion stage was considered as ash. Fixed carbon was determined by subtracting moisture, volatile and ash percentages from 100 %.

The crystalline phases of the samples were identified by X-ray powder diffraction (XRD) using Bruker AXS X-ray diffraction system (model D_2 Phaser SSD160) (Karlsruhe, Germany). The operating voltage and electric current of the X-ray emitter were 30 kV and 10 mA, respectively. Data were collected over the angular range $5 - 80^\circ$ in 2θ under atmospheric pressure for analysis of the crystalline phases.

The morphology of the superactivated hydrochars were observed using a JEOL JSM 6380 L V Scanning Electron Microscope (SEM) (Tokyo, Japan) at magnification of 1200, operating at spot size of 50 at an accelerating voltage of 5 and 10 kV. The samples were observed using SEM as well as characterized elementally using an EDX analyzer (Octane plus, EDAX, USA). Prior to observing under the SEM, all the samples were gold coated in vacuum sputter equipment Denton Vacuum Desk III (Moorestown, NJ).

N_2 adsorption was carried out using High Pressure Volumetric Analyzer (HPVA II, Norcross, GA) to estimate the Brunauer, Emmett, and Teller (BET) surface area, porosity, pore volume. The relative pressure (p/p_o) for N_2 adsorption ranged from 0.009 to 0.995 and a constant temperature of 77 K was maintained using liquid nitrogen. On the other hand, micropore volume and hence micropore area were determined by Dubinin–Astakhov (DA) theory that used CO_2 adsorption isotherms performed in the HPVA II within the pressure range of 0.005–1.11 bar and temperature of 273.15 K. Ultra-high pure nitrogen gas and industrial grade carbon dioxide was used as the adsorption gases in HPVA II. Prior to gas adsorption, the samples were degassed under vacuum at 393 K until the pressure stabilized around 0.6–0.7 Pa to eliminate the eventual fraction of water weakly bound inside the samples. Adsorption data were evaluated using the Microactive software from Micromeritics Instrument Corporation (Norcross, GA). The surface area was calculated using BET method which was applied to adsorption isotherm in the relative pressure range (P/P_o) of 0.05−0.35. Total pore volume was determined using nitrogen adsorption data at close to saturation pressure ($P/P_o \approx 0.99$). Furthermore, the pore size distribution (PSD) was estimated by applying Non-Local Density Functional Theory (NLDFT) to nitrogen adsorption isotherm. Elaboration on determination of micropore structure by applying DA theory on CO_2 adsorption data can be found elsewhere [65].

2.4. Hydrogen adsorption

Hydrogen adsorption experiments were carried out at 77 K of ultra-high purity hydrogen (99.9990 %) using HPVA II automatic adsorption apparatus (Norcross, GA). A 1 cm^3 cell was used as the sample holder in the adsorption experiment. After placing the weighed sample in the holder, the sample was degassed prior to each isothermal measurement in order to remove moisture and adsorbed gases from the surface, as mentioned in material characterization subsection. Sample holder containing the degassed sample was then placed in the liquid-nitrogen-containing dewar (maintaining a temperature of 77 K) and connected to the analysis port of the HPVA II automatic adsorption apparatus. The HPVA II software was used to set pressure steps for adsorption in the range 0.05–2.3 MPa while those for desorption in the range of 2.3 to 0.05 MPa. The generated hydrogen adsorption data were evaluated using Microactive software. The contribution of the empty cell was measured earlier and systematically subtracted to all the generated data in order to improve the accuracy. The Microactive software required packing density as an input value for the total hydrogen uptake determination. Packing density (d_{carbon}) was found using Eq. (1)

$$\text{dcarbon} = \left(\frac{1}{\rho_s} + \text{VT}\right) - 1 \quad (1)$$

Where, ρ_s is the skeletal density (g/cm^3) and V_T (cm^3/g) is the total pore volume that was found from nitrogen adsorption isotherm. Before starting each adsorption test, skeletal density (ρ_s) was determined by using helium adsorption at one pressure point (P = 1 bar). The unit of total hydrogen adsorption (n) measured by HPVA II was in mmol/g. This was then converted to N (wt%) by using Eq. (2). A detailed experimental procedure of hydrogen adsorption can be found elsewhere [66,67].

$$\text{N (wt\%)} = \left(\frac{\frac{n}{1000} \times 2}{1 + \frac{n}{1000} \times 2}\right) \times 100\% \quad (2)$$

3. Results and discussion

3.1. Physiochemical properties of FW, hydrochar, and superactivated hydrochars

In order to probe the effect of HTC and KOH activation on the transformation of FW into suitable porous hydrogen adsorbent materials, physiochemical properties of the samples were investigated in terms of elemental and proximate analyses. The elemental compositions of the studied materials are shown in Table 2. The sulfur content in all the samples were below detection level (0.024 mg). From the same table, the carbon content data clearly shows that the hydrothermal carbonization step of food waste was a means of enriching the carbon prior to activation [41]. Moreover, carbon-rich transformation was also reflected by the decrease of H/C and O/C ratio of FW-Raw while undergoing conversion the HTC process due to dehydration, decarboxylation, and demethanation reactions taking place [68]. On conversion from hydrochar to superactivated hydrochar, dominance of aromatic structure was signified by the overall increase in carbon content while the use of excess KOH eliminated nitrogenous compounds, signified by

Table 2
Proximate and ultimate analysis of biomass, hydrochar and all superactivated hydrochars.

Samples		Proximate Analysis*			Ultimate Analysis*						
	Mass Yield (%)	Volatile Matter (%)	Fixed Carbon (%)	Ash (%)	N (%)	C (%)	H (%)	S (%)	O [a] (%)	O/C	H/C
FW-Raw	100 ± 0.0	69.5 ± 1	23.7 ± 0.1	6.8 ± 0.5	5.8 ± 0.5	47.6 ± 0.5	6.7 ± 0.0	BD**	33.1 ± 0.5	0.78	0.141
FW-HC	23.2 ± 3	56.4 ± 0.1	38.4 ± 0.2	5.2 ± 0.1	6.0 ± 0.6	60.9 ± 0.9	5.2 ± 0.1	BD**	22.7 ± 0.1	0.37	0.085
FW-SAH-R2	21.1 ± 0.6	17.5 ± 0.3	81.6 ± 1	0.9 ± 0.4	1.0 ± 0.2	80.1 ± 2	0.6 ± 0.0	BD**	17.4 ± 0.4	0.22	0.007
FW-SAH-R3	16.5 ± 0.9	16.4 ± 0.2	80.7 ± 0.1	2.9 ± 0.2	1.4 ± 0.6	83.3 ± 1	0.5 ± 0.0	BD**	11.9 ± 0.4	0.14	0.006
FW-SAH-R4	12.9 ± 1.0	15.5 ± 0.5	79.6 ± 1	4.9 ± 0.1	1.0 ± 0.3	85.1 ± 1	0.4 ± 0.2	BD**	8.6 ± 0.5	0.10	0.005

** Below detection limit.
[a] The O content determined by the difference method.

the overall decrease of nitrogen content [69]. On the other hand, while undergoing the activation process, increasing weight ratios of KOH/ hydrochar from 2 to 4, the carbon content increased from 80.1–85.1%, whereas the H and O content decreased from 0.6 to 0.4 % and 17.4–8.6%, respectively. This expected change, owing to the activation process, is also reflected in the minor values of O/C factor. The significant decrease in the O/C and H/C value of the superactivated hydrochars from the non-activated hydrochar value signifies the aromaticity development in the superactivated hydrochar due to removing of H and O from inside the material [70–73].

From Table 2, HTC at 220 °C of FW-raw resulted in small amount of solid hydrochar yield (23.2 %) which could be because of primary or secondary decomposition of biomass or solid residue, respectively [74]. Literature reported mass yield for such food waste undergoing HTC at an alike temperature ranged from 7% to 32.5 % [60,62]. On the other hand, mass yield of FW−HC undergoing activation decreased from 21.1 % with the increase of KOH: hydochar ratio which could be attributed to the larger surface area of the corresponding superactivated hydrochars. During the chemical activation, with the increase of KOH, more carbon atoms are oxidized that eventually leads to more pore formation and hence greater porosity is developed at the expense of char burn off [75,76]. In fact, several studies revealed a low mass yield for such activating conditions that vary between 17%–31% [77]. In addition, using proximate analysis data of Table 2, the volatile matters in the FW−HC (56.4 %) is significantly lower than that in the FW-Raw (69.5 %) which was due to their loss in the gaseous and liquid phases during the HTC process [78–81]. In case of superactivated hydrochar, the release of H_2O, CO_2 and CO during the activation process lead to the development of porous tunnels which resulted in further decrease of volatile matter [82]. Also from the same table, the ash content of the samples was in the range of 6.8−4.9%. Undergoing HTC, ash content was reduced by 23.5 % where a similar transition was observed by Saqib et al. [60] where 29.5 % reduction of ash took place for food waste undergoing HTC at 200 °C. On KOH activation of hydrochar, ash content followed an increasing trend (0.9%–4.9%) with the activating agent ratio as similarly concluded by Hassen [83]. The increment could be explained by the effect of activating agent residue during the washing step which was also evident with the increasing amount of surface potassium content from 15.7 wt% to 30.6 wt%, as shown in Table S1 (Supplementary document). Moreover, presence of copper, chlorine as well as silica was observed among the inorganic constituents of the superactivted hydrochars where appearance of silica in the superactivated hydrochars might be due to the use of quartz crucible during activation. However, the ash content of the superactivated hydrochars was within commercially acceptable value of 5 wt% [84].

3.2. Surface morphology alteration from FW to superactivated hydrochars

In context with the above discussion (Section 3.1), metamorphosis of the physicochemical properties in FW as it underwent HTC and KOH activation implicated the development of porosity in the superactivated hydrochars. However, to be useful as hydrogen storage materials, the substantial development of porosity needs to be quantified and compared. Hence, porosity of the materials was probed, and surface morphology of the studied materials were investigated in terms of surface area, pore properties, and crystallinity. The surface area and pore properties of the materials are shown in Table 3.

The surface area of FW-Raw and FW−HC were 0.24 and 1.32 m^2/g, respectively. Generally, availability of surface porosity values for biomass is limited due to the lack of considerable pores in it whereas the surface area of FW−HC was similar to the literature value where food-waste pyrolyzed char had surface area of 1.9 m^2/g [48,85]. Such low surface area mainly results from interparticle voids [86]. Although, FW-Raw and FW−HC have low surface areas and insignificant pore properties, the redox reactions of hydrochar with KOH resulted in a noteworthy improvement of the BET surface area and the total pore volume, which ranged from 2068 to 2885 m^2/g and 0.98 to 1.93 cm^3/g, respectively. The reaction between the carbonaceous material (hydrochar) and the activating agent (KOH) results in the reduction of potassium which then intercalates between carbon layers of hydrochar and expand the carbon lattice to create porosity. The elaborated reaction mechanism is found in elsewhere [87,88]. Along with the increase of KOH/ hydrochar mass ratio, more pores are generated as the spacers that interconnect the carbon nanorods are all etched by KOH which consequently increases surface area and pore volume [89]. Total pore volume increased from 0.98 to 1.93 cm^3/g with the increase of KOH/ hydrochar ratio also reflecting the increase of micropore volume from 0.95 to 0.60 cm^3/g. However, decrease in the micropore volume fraction (a ratio between total pore volume and micropore volume) from 0.95 to 0.60 was observed which could be due to the over-exfoliation with increasing weight ratios of KOH/ hydrochar that ultimately resulted in overall pore development but the proportion of micropores fell.

Table 3
Pore texture parameters of AC derived from N_2 adsorption-desorption data.

Sample	BET surface Area (m^2/g)	Total pore volume (cm^3/g)	Micropore surface area (m^2/g)	Micropore volume (cm^3/g)	Micropore volume fraction[#]
FW-RAW	0.24 ± 0.01	a*	BD**	BD**	N/A
FW-HC	1.32 ± 0.03	b*	BD**	BD**	N/A
FW-SAH-R2	2068 ± 60	0.98	1353	0.94	0.95
FW-SAH-R3	2791 ± 28	1.71	2109	1.34	0.79
FW-SAH-R4	2885 ± 17	1.93	1634	1.15	0.60

a = 0.000338.
b = 0.001674.
[#] Micropore volume fraction $= \frac{\text{Micropore volume}}{\text{Total pore volume}}$.
* Values rounded off to two decimal place.
** Below detection limit.

Several authors reported parallel results about the effect of activation ratio [50,57,90], for example, Wróbel-Iwaniec et al. derived porous carbon from chitosan and observed increased surface area and pore volume from 1926 to 2840 m^2/g and 0.82 to 1.25 cm^3/g respectively with the increase of activation ratio from 2 to 4 whereas the micropore volume ratio decreased by 10.9 % [50].

The development of porosity in the superactivated hydrochars derived from the food waste could be observedfrom the N_2 adsorption isotherms shown in Fig. 1. From Fig. 1(a), the N_2 adsorption isotherms for FW-Raw and FW−HC show very low quantity of N_2 adsorbed, signifying negligible porosity. On the other hand, N_2 adsorption isotherms of the superactivated hydrochar- FW-SAH-R2- show a sharp increase in the quantity of N_2 adsorbed that occurs at a very low relative pressures (lower than 0.05), and then plateaus at higher pressures, indicating isotherm type I according to International Union of Pure and Applied Chemistry (IUPAC) classification [91] which signifies the predominance of microporosity in the superactivated hydrochar [92]. As the KOH/hydrochar ratio is increased from 2:1 to 3:1 and 4:1, there is a distinct widening of the isotherms for both 3:1 and 4:1 which indicates the widening of micropore for the development of some mesoporosity, which is well explained for the activation mechanism [93].

Fig. 1(b) shows the pore size distribution (PSD) of food waste biomass, hydrochar and superactivated hydrochars calculated by the nonlocal density functional theory (NLDFT) model. For the FW-Raw and FW−HC, it is evident from PSD that despite negligible pore development, presumably some voids were detected as pores in the size range of 14 − 16 nm that exist in the volume of 0.0003 and 0.0017 cm^3/g respectively. On the other hand, in case of superactivated hydrochars, a large proportion of pores lie between 1 − 2 nm (1 nm = 10 Å). In correspondence to the broadening of the isotherm knees for superactivated hydrochars of KOH/ hydrochar ratio 3:1 and 4:1, the PSD shows mesopores evolution, significant in pore fraction for the pore size of 2 − 5 nm, as such small mesopores contribute notably in high-pressure hydrogen storage [50,57,94–96]. Balathanigaimani et al. reported an increase of average pore width from 1.65 to 2.50 nm on increasing activation ratio from 2 to 4 [50]. From the transition of food waste's surface morphology is more distinctly highlighted in the SEM images. Food waste, with no pores as seen in Fig. 2(a), underwent hydrothermal carbonization that might had initiated 'spores' like surface development which still had negligible 'pores' in the resulting hydrochar (Fig. 2(b)). On activation, evolution of numerous pores can be seen on the surface for all the superactivated hydrochars (Fig. 2(b), (c) and (d)) while comparatively more number of smaller pores might had evolved in FW-SAH-R2 whereas more number of pores might be developed in FW-SAH-R4 as also found corresponding to the total pore volume data in Table 3.

For further investigation of the surface morphology (e.g., crystallinity), XRD of the samples were conducted which is shown in Fig. 3. In case of FW-Raw and FW−HC, a broad diffraction peak at 2θ range of 12 − 28 ° was observed, which signifies non-graphitic structure of the carbon material [97]. The disappearance of 2θ peak at 20 ° for FW−HC attributes to the disappearance of microcrystalline structure of FW-Raw after HTC [98]. This was expected because the hydrochar, by definition, has an amorphous structure [99]. The broad reflection at 2θ around 20 ° in the hydrochar sample could be due to the interlayer (002) reflections among irregular polycyclic aromatic sheets of amorphous carbon [100]. The peaks present in the hydrochar can be attributed to the presence of impurities in the structure [73]. XRD patterns of the superactivated hydrochar samples presented broad peak at ~24 ° corresponds to (002) plane and that of at ~44 ° corresponds to (100/101) plane that are characteristic of typical amorphous graphite crystal structure with very low long-range order degree [101]. In addition, the presence of a large number of microporous structure in the superactivated hydrochar samples are reflected in the high intensity peaks in the low angle region (5−15 °) [101].

3.3. Hydrogen gas storage capacity of FW derived superactivated hydrochar

The above discussed results of superior surface porosity reassured the feasibility of implementing the superactivated hydrochars for the purpose of hydrogen storage. SEM images in Fig. 2 illustrates the surface appearance of more finely developed pores which support the increasing hydrogen capacity that is exhibited by the materials with increased weight ratios of KOH/ hydrochar. The gravimetric (wt%) hydrogen uptake by the superactivated hydrochars at high pressure was analyzed and graphically presented in Fig. 4 where hydrogen adsorption isotherms of FW-RAW and FW−HC was not included as it demonstrated negligible hydrogen storage owing to the insignificant surface porosity. The hydrogen adsorption isotherms at 77 K from 0–23 bar show broad knee which signifies the gradual increment of hydrogen uptake with pressure up to 23 bar, without a clear plateau at the low-pressure range (0–1 bar), signifying more available room for hydrogen adsorption by the materials. On the other hand, the initial steeper adsorption isotherm corresponding to KOH/ hydrochar ratio of 2:1 is explained by the higher proportion of micropore in that superactivated hydrochar material. In addition, hydrogen storage capacity increased with weight ratios of KOH/ hydrochar in all the experimental pressure ranges where hydrogen storage at the maximum pressure of 23 bar also increased from 4.53 to 6.15 wt% with the increase of KOH/ hydrochar from 2:1 to 4:1, respectively. Inclusive of data from Table 3, it can be observed that higher BET surface area and total pore volume synergistically played a positive role in substantially increasing the hydrogen adsorbed quantity with increase of KOH/ hydrochar which was expected. This was because hydrogen adsorption capacity is governed by the factors which affect adsorbate-adsorbent interactions and one of the overriding factors

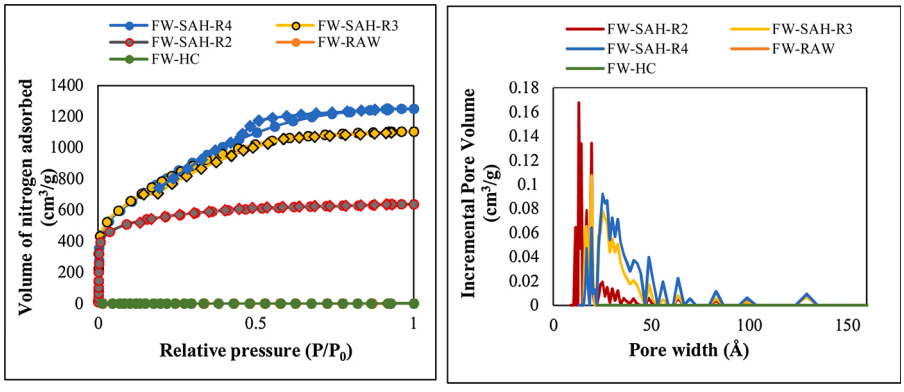

Fig. 1. (a) Nitrogen adsorption-desorption isotherms of investigated superactivated hydrochars at 77 K as a function of relative pressure. (b) Pore size distribution calculated from the NLDFT model.

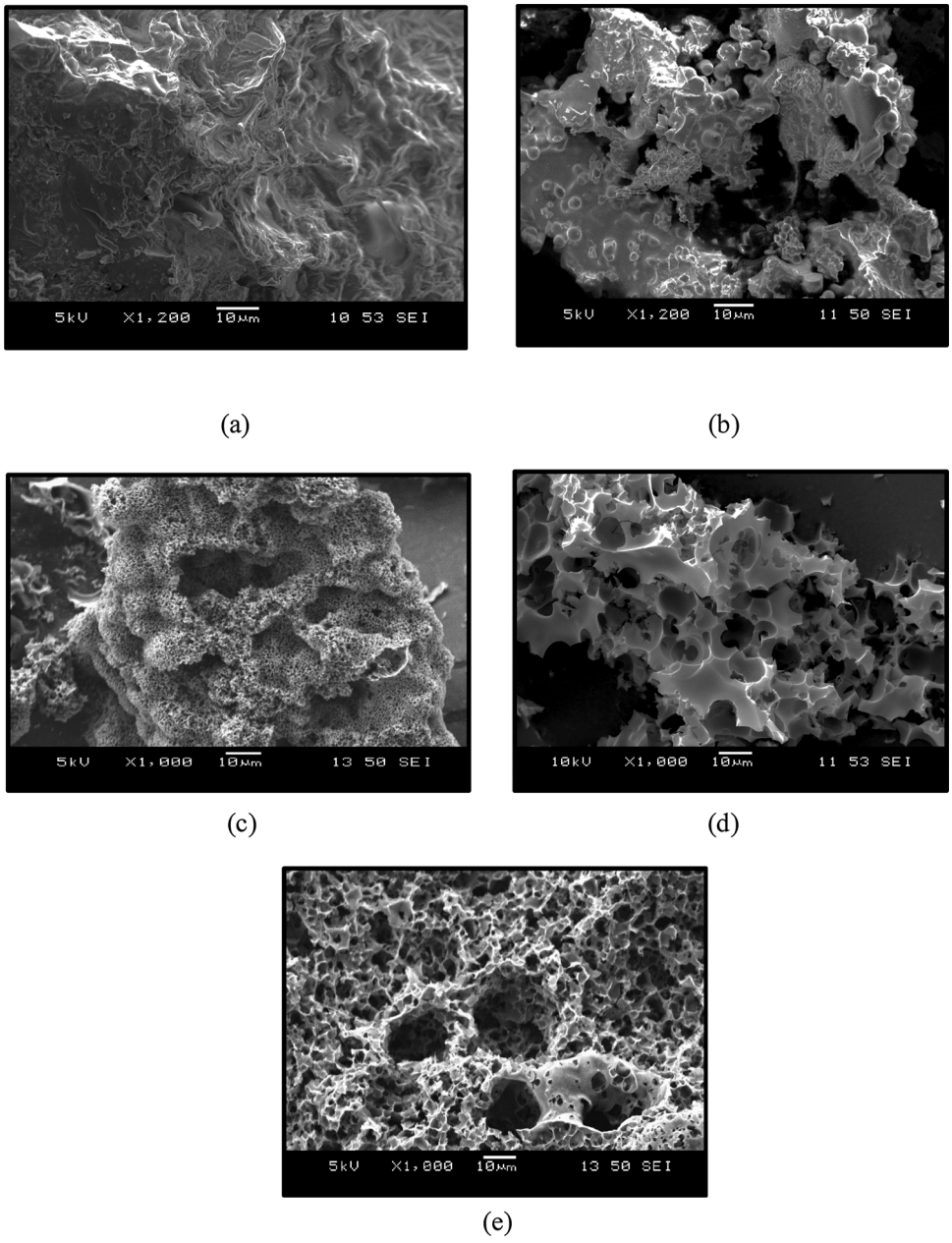

Fig. 2. SEM images of (a) FW-Raw, (b) FW−HC, (c) FW-SAH-R2, (d) FW-SAH-R3, and (e) FW-SAH-R4.

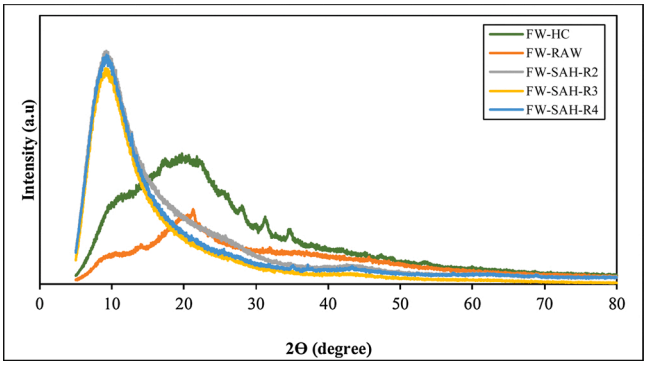

Fig. 3. XRD pattern of biomass, hydrochar and all superactivated hydrochars.

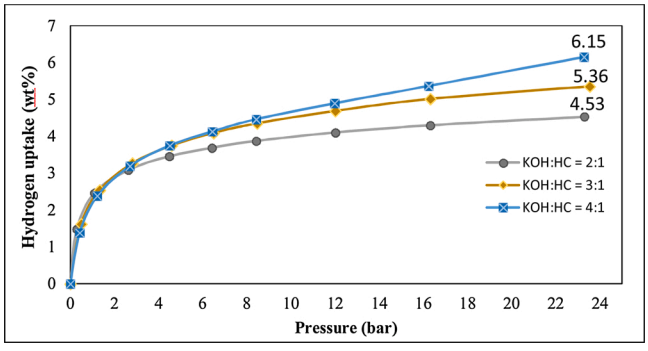

Fig. 4. Hydrogen adsorption isotherms at 77 K up to 23 bar where KOH: HC denotes KOH/ hydrochar ratio.

include surface area and pore volume [48,50,82,95]. The mechanism for hydrogen storage by means of physisorption is the van der Waals attraction between the surface of the adsorbent and hydrogen molecules [102]. As the van der Waals interaction between hydrogen molecules is weak, to expect a few layers of hydrogen packing on an adsorbent surface is impractical [103]. Therefore, hydrogen adsorption on the adsorbent is a monolayer and large surface area is found to be beneficial for higher uptake.

Moreover, along with increase of the pressure, hydrogen adsorbed in the micropores tends to saturated and the small mesopores between 2 and 5 nm then become the primary hosts for hydrogen uptake that further facilitates hydrogen adsorption [95,104]. Therefore, from Fig. 4 it can be inferred that better hydrogen storage capacity was reflected for KOH: HC = 2 in the low pressure range of upto 2 bar than the other superactivated hydrochars, owing to the former's higher micropore volume fraction. Similar observation was equated from Table 3 where the micropore volume fraction decreased from 0.95 to 0.60 with the amount of KOH used that corresponds to an increase in the respective mesopore volume fraction and hence a possible reason behind increasing hydrogen uptake at high pressure. Hydrogen adsorption capacity of material with comparable surface area of 1930 and 2835 m^2/g derived from sword-bean shells and wood chips respectively showed cryogenic hydrogen uptake of 3.8 wt% and 6.4 wt% at relatively higher pressure of 40 and 80 bar respectively [73,96]. The better hydrogen adsorption capacity of food waste derived superactivated hydrochar might be attributed to its superior total pore volume which complies with findings in literature that ascertains roughly linear correlations of hydrogen uptake with total pore volume [50,95]. On the other hand, for model compound of cellulose acetate that underwent analogous HTC and activation process conditions, Blankenship et al. [7] reported cryogenic hydrogen uptake capacity of 6.8 wt% at 20 bar. The superior hydrogen storage capacity could be explained by the combination of high surface area reported to be as 2864 m^2/g in addition to almost 0.9 micropore volume fraction, where ultra-micropores of 6−7 Å were present, which could therefore enhance hydrogen storage capacity at both high and low pressure respectively [7].

4. Conclusion

It can be concluded from this study that due to the abundance of food waste as well as possible development of favorable porosity in the food waste derived superactivated hydrochars, food waste can be considered as an excellent candidate to synthesize hydrogen gas adsorbent via the process of hydrothermal carbonization followed by chemical activation (using KOH). In addition, surface area and total pore volume synergistically enhanced hydrogen uptake capacity of the developed superactivated hydrochars. Porosity of the developed materials were significantly improved by increasing the ratio of hydrochar to the activating agent where the obtained surface area and total pore volume were maximum of 2885 m^2/g and 1.93 cm^3/g respectively for the superactivated hydrochar prepared at KOH/hydrochar ratio of 4:1 and the corresponding hydrogen adsorbed was noted to be the highest of 6.15 wt% at 23 bar. Therefore, from the results it can be also suggested that the as-prepared porous carbon material is comparable or better than those reported in the open literature for hydrogen adsorption purpose and this demonstrates to be an effective route of developing applicable hydrogen storage material from food waste. In addition, while the target of US Department of Energy (DOE) gravimetric hydrogen storage capacity (2020) was 4.3 wt% at a maximum delivery pressure of 12 bar and minimum operating temperature of 233 K [105], this study revealed hydrogen storage capacity of 4.9 wt% at 12 bar and at lower temperature of 77 K in superactivated hydrochars derived from food waste which was certainly a step towards achieving DOE's goal.

Authorship statement

Sultana, A.I.: Conception and design of study, acquisition of data, data analysis, drafting manuscript, revising manuscript based on reviewer comments

Saha, N.: Data analysis, manuscript revision

Reza, M.T.: Conception and design of study, funding acquisition, manuscript revision

Declaration of Competing Interest

The authors declare that they have no known competing financial interests or personal relationships that could have appeared to influence the work reported in this paper.

Acknowledgement

The research is funded by the United States Department of Agriculture (USDA) grant (2019-67019-2928) and National Science Foundation grant (1856058). The authors acknowledge Tatiana Karpova of SEM Lab, undergraduate students Cadianne Chambers and Mathew Harvey as well as graduate students Kyle McGaughy, Md. Tahmid Islam, and Thomas Quaid from Biofuels lab at Florida Institute of Technology for their valuable inputs in the manuscript to make it more organized.

Appendix A. Supplementary data

Supplementary material related to this article can be found, in the online version, at doi:https://doi.org/10.1016/j.jaap.2021.105322.

References

[1] F & Sullivan, Hydrogen Production to Double by 2030 as the World Advances towards a Sustainable Energy Economy, (n.d.). https://www.prnewswire.com/news-releases/hydrogen-production-to-double-by-2030-as-the-world-advances-towards-a-sustainable-energy-economy-301169453.html (accessed March 7, 2021).
[2] The Future of Hydrogen – Analysis, IEA. (n.d.). https://www.iea.org/reports/the-future-of-hydrogen (accessed March 7, 2021).
[3] N. Demirdöven, J. Deutch, Hybrid cars now, fuel cell cars later, Science 305 (2004) 974–976, https://doi.org/10.1126/science.1093965.
[4] P. Moriarty, D. Honnery, Hydrogen's role in an uncertain energy future, Int. J. Hydrogen Energy 34 (2009) 31–39.
[5] J.A. Turner, A realizable renewable energy future, Science 285 (1999) 687–689.
[6] L. Schlapbach, A. Züttel, Hydrogen-storage materials for mobile applications. Materials for Sustainable Energy: a Collection of Peer-reviewed Research and Review Articles From Nature Publishing Group, World Scientific, 2011, pp. 265–270.
[7] T.S. Blankenship Ii, N. Balahmar, R. Mokaya, Oxygen-rich microporous carbons with exceptional hydrogen storage capacity, Nat. Commun. 8 (2017) 1545, https://doi.org/10.1038/s41467-017-01633-x.
[8] K.T. Møller, T.R. Jensen, E. Akiba, H. Li, Hydrogen - A sustainable energy carrier, Progress in Natural Sci.: Mater. Int. 27 (2017) 34–40, https://doi.org/10.1016/j.pnsc.2016.12.014.
[9] ROAD MAP TO A US HYDROGEN ECONOMY, (n.d.). https://cafcp.org/sites/default/files/Road%2BMap%2Bto%2Ba%2BUS%2BHydrogen%2BEconomy%2BFull%2BReport.pdf (accessed November 9, 2020).
[10] C. Koroneos, A. Dompros, G. Roumbas, Hydrogen production via biomass gasification—a life cycle assessment approach, Chem. Eng. Process. Process. Intensif. 47 (2008) 1261–1268, https://doi.org/10.1016/j.cep.2007.04.003.
[11] C.M. Kalamaras, A.M. Efstathiou, Hydrogen production technologies: current State and future developments, Conference Papers in Energy (2013) e690627, https://doi.org/10.1155/2013/690627, 2013.
[12] J.A. Turner, Sustainable hydrogen production, Science 305 (2004) 972–974, https://doi.org/10.1126/science.1103197.
[13] I.K. Kapdan, F. Kargi, Bio-hydrogen production from waste materials, Enzyme Microb. Technol. 38 (2006) 569–582, https://doi.org/10.1016/j.enzmictec.2005.09.015.
[14] I. Dincer, C. Acar, Review and evaluation of hydrogen production methods for better sustainability, Int. J. Hydrogen Energy 40 (2015) 11094–11111, https://doi.org/10.1016/j.ijhydene.2014.12.035.
[15] C. Acar, I. Dincer, Comparative assessment of hydrogen production methods from renewable and non-renewable sources, Int. J. Hydrogen Energy 39 (2014) 1–12, https://doi.org/10.1016/j.ijhydene.2013.10.060.

[16] R. Kothari, D. Buddhi, R.L. Sawhney, Comparison of environmental and economic aspects of various hydrogen production methods, Renewable Sustainable Energy Rev. 12 (2008) 553–563, https://doi.org/10.1016/j.rser.2006.07.012.

[17] P. Nikolaidis, A. Poullikkas, A comparative overview of hydrogen production processes, Renewable Sustainable Energy Rev. 67 (2017) 597–611, https://doi.org/10.1016/j.rser.2016.09.044.

[18] J.D. Holladay, J. Hu, D.L. King, Y. Wang, An overview of hydrogen production technologies, Catal. Today 139 (2009) 244–260.

[19] E. Kırtay, Recent advances in production of hydrogen from biomass, Energy Convers. Manage. 52 (2011) 1778–1789, https://doi.org/10.1016/j.enconman.2010.11.010.

[20] M. Sevilla, R. Mokaya, Energy storage applications of activated carbons: supercapacitors and hydrogen storage, Energy Environ. Sci. 7 (2014) 1250–1280.

[21] N. Bader, A. Ouederni, Optimization of biomass-based carbon materials for hydrogen storage, J. Energy Storage 5 (2016) 77–84, https://doi.org/10.1016/j.est.2015.12.009.

[22] D. Sadoway, The missing link to renewable energy Youtube Video, (n.d.).

[23] E. Uçkun Kiran, A.P. Trzcinski, W.J. Ng, Y. Liu, Bioconversion of food waste to energy: a review, Fuel 134 (2014) 389–399, https://doi.org/10.1016/j.fuel.2014.05.074.

[24] Global food wastage could hit 2.1 billion tons by 2030 in “staggering” crisis, (2018). https://www.consulting.us/news/860/global-food-wastage-could-hit-21-billion-tons-by-2030-in-staggering-crisis (accessed January 8, 2021).

[25] FAO - News Article: Food wastage: Key facts and figures, (n.d.). http://www.fao.org/news/story/en/item/196402/icode/ (accessed February 19, 2021).

[26] O. US EPA, Advancing Sustainable Materials Management: Facts and Figures Report, EPA, US, 2015 (accessed January 8, 2021), https://www.epa.gov/facts-and-figures-about-materials-waste-and-recycling/advancing-sustainable-materials-management.

[27] Food Waste in America in 2020: Statistics & Facts | RTS, Recycle Track Systems. (n.d.). https://www.rts.com/resources/guides/food-waste-america/ (accessed January 8, 2021).

[28] Estimation of the Moisture Content in Typical MSW, (n.d.) 11.

[29] S. Otles, S. Despoudi, C. Bucatariu, C. Kartal, Chapter 1 - food waste management, valorization, and sustainability in the food industry, in: C.M. Galanakis (Ed.), Food Waste Recovery, Academic Press, San Diego, 2015, pp. 3–23, https://doi.org/10.1016/B978-0-12-800351-0.00001-8.

[30] Profiles in Garbage: Food Waste, Waste360, 2000 (accessed February 5, 2021), https://www.waste360.com/mag/waste_profiles_garbage_food.

[31] Z. Liu, R. Balasubramanian, Hydrothermal carbonization of waste biomass for energy generation, Procedia Environ. Sci. 16 (2012) 159–166, https://doi.org/10.1016/j.proenv.2012.10.022.

[32] T.P.T. Pham, R. Kaushik, G.K. Parshetti, R. Mahmood, R. Balasubramanian, Food waste-to-energy conversion technologies: current status and future directions, Waste Manag. 38 (2015) 399–408, https://doi.org/10.1016/j.wasman.2014.12.004.

[33] A. Funke, F. Ziegler, Hydrothermal carbonization of biomass: a summary and discussion of chemical mechanisms for process engineering, Biofuels, Bioproducts and Biorefining. 4 (2010) 160–177, https://doi.org/10.1002/bbb.198.

[34] M.T. Reza, J. Andert, B. Wirth, D. Busch, J. Pielert, J. Lynam, J. Mumme, Review Article: Hydrothermal Carbonization of Biomass for Energy and Crop Production, Appl. Bioenergy 1 (2014), https://doi.org/10.2478/apbi-2014-0001.

[35] O. Arellano, M. Flores, J. Guerra, A. Hidalgo, D. Rojas, A. Strubinger, Hydrothermal carbonization of corncob and characterization of the obtained hydrochar, Chem. Eng. Res. Des. 50 (2016) 235–240, https://doi.org/10.3303/CET1650040.

[36] N. Saha, K. McGaughy, M.T. Reza, Elucidating hydrochar morphology and oxygen functionality change with hydrothermal treatment temperature ranging from subcritical to supercritical conditions, J. Anal. Appl. Pyrolysis 152 (2020) 104965, https://doi.org/10.1016/j.jaap.2020.104965.

[37] N. Saha, A. Saba, M.T. Reza, Effect of hydrothermal carbonization temperature on pH, dissociation constants, and acidic functional groups on hydrochar from cellulose and wood, J. Anal. Appl. Pyrolysis 137 (2019) 138–145, https://doi.org/10.1016/j.jaap.2018.11.018.

[38] M. Sevilla, A.B. Fuertes, The production of carbon materials by hydrothermal carbonization of cellulose, Carbon 47 (2009) 2281–2289, https://doi.org/10.1016/j.carbon.2009.04.026.

[39] M. Sevilla, A.B. Fuertes, Chemical and structural properties of carbonaceous products obtained by hydrothermal carbonization of Saccharides, Chem. Eur. J. 15 (2009) 4195–4203, https://doi.org/10.1002/chem.200802097.

[40] M. Sevilla, A.B. Fuertes, R. Mokaya, High density hydrogen storage in superactivated carbons from hydrothermally carbonized renewable organic materials, Energy Environ. Sci. 4 (2011) 1400–1410, https://doi.org/10.1039/C0EE00347F.

[41] W. Sangchoom, R. Mokaya, Valorization of lignin waste: carbons from hydrothermal carbonization of renewable lignin as superior sorbents for CO2 and hydrogen storage, ACS Sustainable Chem. Eng. 3 (2015) 1658–1667, https://doi.org/10.1021/acssuschemeng.5b00351.

[42] M. Sevilla, R. Mokaya, A.B. Fuertes, Ultrahigh surface area polypyrrole-based carbons with superior performance for hydrogen storage, Energy Environ. Sci. 4 (2011) 2930–2936, https://doi.org/10.1039/C1EE01608C.

[43] J.A. Maciá-Agulló, B.C. Moore, D. Cazorla-Amorós, A. Linares-Solano, Activation of coal tar pitch carbon fibres: physical activation vs. Chemical activation, Carbon 42 (2004) 1367–1370, https://doi.org/10.1016/j.carbon.2004.01.013.

[44] M. Wu, Q. Zha, J. Qiu, Y. Guo, H. Shang, A. Yuan, Preparation and characterization of porous carbons from PAN-based preoxidized cloth by KOH activation, Carbon 42 (2004) 205–210, https://doi.org/10.1016/j.carbon.2003.10.025.

[45] D. Lozano-Castelló, D. Cazorla-Amorós, A. Linares-Solano, Can highly activated carbons be prepared with a homogeneous micropore size distribution? Fuel Process. Technol. 77–78 (2002) 325–330, https://doi.org/10.1016/S0378-3820(02)00048-6.

[46] M. Kılıç, E. Apaydın-Varol, A.E. Pütün, Preparation and surface characterization of activated carbons from Euphorbia rigida by chemical activation with ZnCl2, K2CO3, NaOH and H3PO4, Appl. Surf. Sci. 261 (2012) 247–254, https://doi.org/10.1016/j.apsusc.2012.07.155.

[47] J. Wang, S. Kaskel, KOH activation of carbon-based materials for energy storage, J. Mater. Chem. 22 (2012) 23710–23725.

[48] A.I. Sultana, N. Saha, M.T. Reza, Synopsis of factors affecting hydrogen storage in biomass-derived activated carbons, Sustainability 13 (2021) 1947, https://doi.org/10.3390/su13041947.

[49] Preparation of activated carbons from Spanish anthracite. I. Activation by KOH, Fuel Energy Abstr. 43 (2002) 110, https://doi.org/10.1016/S0140-6701(02)85178-5.

[50] I. Wróbel-Iwaniec, N. Díez, G. Gryglewicz, Chitosan-based highly activated carbons for hydrogen storage, Int. J. Hydrogen Energy 40 (2015) 5788–5796, https://doi.org/10.1016/j.ijhydene.2015.03.034.

[51] A. Linares-Solano, D. Lozano-Castelló, M.A. Lillo-Ródenas, D. Cazorla-Amorós, Carbon activation by alkaline hydroxides preparation and reactions, porosity and performance, Chem. Phys. Carbon. 30 (2008) 1–62.

[52] M.J.B. Evans, E. Halliop, J.A.F. MacDonald, The production of chemically-activated carbon, Carbon 37 (1999) 269–274, https://doi.org/10.1016/S0008-6223(98)00174-2.

[53] Y. Sudaryanto, S.B. Hartono, W. Irawaty, H. Hindarso, S. Ismadji, High surface area activated carbon prepared from cassava peel by chemical activation, Bioresour. Technol. 97 (2006) 734–739, https://doi.org/10.1016/j.biortech.2005.04.029.

[54] M.A. Lillo-Ródenas, J. Juan-Juan, D. Cazorla-Amorós, A. Linares-Solano, About reactions occurring during chemical activation with hydroxides, Carbon 42 (2004) 1371–1375, https://doi.org/10.1016/j.carbon.2004.01.008.

[55] J. Wang, I. Senkovska, S. Kaskel, Q. Liu, Chemically activated fungi-based porous carbons for hydrogen storage, Carbon 75 (2014) 372–380, https://doi.org/10.1016/j.carbon.2014.04.016.

[56] Y.-J. Heo, S.-J. Park, Synthesis of activated carbon derived from rice husks for improving hydrogen storage capacity, J. Ind. Eng. Chem. 31 (2015) 330–334, https://doi.org/10.1016/j.jiec.2015.07.006.

[57] Y. Xiao, H. Dong, C. Long, M. Zheng, B. Lei, H. Zhang, Y. Liu, Melaleuca bark based porous carbons for hydrogen storage, Int. J. Hydrogen Energy 39 (2014) 11661–11667, https://doi.org/10.1016/j.ijhydene.2014.05.134.

[58] J. Jiang, Y. Zhang, K. Li, Q. Wang, C. Gong, M. Li, Volatile fatty acids production from food waste: effects of pH, temperature, and organic loading rate, Bioresour. Technol. 143 (2013) 525–530, https://doi.org/10.1016/j.biortech.2013.06.025.

[59] A.R. Maag, A.D. Paulsen, T.J. Amundsen, P.E. Yelvington, G.A. Tompsett, M. T. Timko, Catalytic hydrothermal liquefaction of food waste using CeZrOx, Energies 11 (2018) 564, https://doi.org/10.3390/en11030564.

[60] N.U. Saqib, S. Baroutian, A.K. Sarmah, Physicochemical, structural and combustion characterization of food waste hydrochar obtained by hydrothermal carbonization, Bioresour. Technol. 266 (2018) 357–363, https://doi.org/10.1016/j.biortech.2018.06.112.

[61] D.P. Komilis, R.K. Ham, Carbon dioxide and ammonia emissions during composting of mixed paper, yard waste and food waste, Waste Manag. 26 (2006) 62–70.

[62] S. Mazumder, P. Saha, M.T. Reza, Co-hydrothermal carbonization of coal waste and food waste: fuel characteristics, Biomass Conv. Bioref. (2020), https://doi.org/10.1007/s13399-020-00771-5.

[63] L. Chunlan, X. Shaoping, G. Yixiong, L. Shuqin, L. Changhou, Effect of pre-carbonization of petroleum cokes on chemical activation process with KOH, Carbon 43 (2005) 2295–2301, https://doi.org/10.1016/j.carbon.2005.04.009.

[64] Analysis of Oxygen, Oxygen Content of Biomass - Celignis Biomass Analysis Laboratory, (n.d.). https://www.celignis.com/analyte.php?value=26 (accessed March 8, 2021).

[65] C. Wedler, R. Span, Micropore analysis of biomass chars by CO2 adsorption: comparison of different analysis methods, Energy Fuels 35 (2021) 8799–8806, https://doi.org/10.1021/acs.energyfuels.1c00280.

[66] S. Schaefer, A. Jeder, G. Sdanghi, P. Gadonneix, A. Abdedayem, M.T. Izquierdo, G. Maranzana, A. Ouederni, A. Celzard, V. Fierro, Oxygen-promoted hydrogen adsorption on activated and hybrid carbon materials, Int. J. Hydrogen Energy 45 (2020) 30767–30782, https://doi.org/10.1016/j.ijhydene.2020.08.114.

[67] L. Giraldo, J.C. Moreno-Piraján, Exploring the use of rachis of chicken feathers for hydrogen storage, J. Anal. Appl. Pyrolysis 104 (2013) 243–248, https://doi.org/10.1016/j.jaap.2013.07.009.

[68] A.B. Fuertes, M.C. Arbestain, M. Sevilla, J.A. Maciá-Agulló, S. Fiol, R. López, R. J. Smernik, W.P. Aitkenhead, F. Arce, F. Macìas, Chemical and structural properties of carbonaceous products obtained by pyrolysis and hydrothermal carbonisation of corn stover, Soil Res. 48 (2010) 618–626.

[69] E. Yagmur, M. Ozmak, Z. Aktas, A novel method for production of activated carbon from waste tea by chemical activation with microwave energy, Fuel 87 (2008) 3278–3285, https://doi.org/10.1016/j.fuel.2008.05.005.

[70] K.A. Spokas, Review of the stability of biochar in soils: predictability of O:C molar ratios, Carbon Manag. 1 (2010) 289–303, https://doi.org/10.4155/cmt.10.32.

[71] S. Maisano, F. Urbani, N. Mondello, V. Chiodo, Catalytic pyrolysis of Mediterranean sea plant for bio-oil production, Int. J. Hydrogen Energy 42 (2017) 28082–28092, https://doi.org/10.1016/j.ijhydene.2017.07.124.
[72] S. Cataldo, V. Chiodo, F. Crea, S. Maisano, D. Milea, A. Pettignano, Biochar from byproduct to high value added material – a new adsorbent for toxic metal ions removal from aqueous solutions, J. Mol. Liq. 271 (2018) 481–489, https://doi.org/10.1016/j.molliq.2018.09.009.
[73] R. Pedicini, S. Maisano, V. Chiodo, G. Conte, A. Policicchio, R.G. Agostino, Posidonia Oceanica and Wood chips activated carbon as interesting materials for hydrogen storage, Int. J. Hydrogen Energy 45 (2020) 14038–14047, https://doi.org/10.1016/j.ijhydene.2020.03.130.
[74] G.K. Parshetti, S. Kent Hoekman, R. Balasubramanian, Chemical, structural and combustion characteristics of carbonaceous products obtained by hydrothermal carbonization of palm empty fruit bunches, Bioresour. Technol. 135 (2013) 683–689, https://doi.org/10.1016/j.biortech.2012.09.042.
[75] H.P.S. Abdul Khalil, P. Firoozian, I.O. Bakare, H.Md. Akil, A.Md. Noor, Exploring biomass based carbon black as filler in epoxy composites: flexural and thermal properties, Mater. Des. 31 (2010) 3419–3425, https://doi.org/10.1016/j.matdes.2010.01.044.
[76] A.S. Mestre, A.S. Bexiga, M. Proença, M. Andrade, M.L. Pinto, I. Matos, I. M. Fonseca, A.P. Carvalho, Activated carbons from sisal waste by chemical activation with K2CO3: kinetics of paracetamol and ibuprofen removal from aqueous solution, Bioresour. Technol. 102 (2011) 8253–8260, https://doi.org/10.1016/j.biortech.2011.06.024.
[77] T.S. Hui, M.A.A. Zaini, Potassium hydroxide activation of activated carbon: a commentary, Carbon Lett. 16 (2015) 275–280, https://doi.org/10.5714/CL.2015.16.4.275.
[78] N. Kobayashi, N. Okada, A. Hirakawa, T. Sato, J. Kobayashi, S. Hatano, Y. Itaya, S. Mori, Characteristics of solid residues obtained from hot-compressed-Water treatment of woody biomass, Ind. Eng. Chem. Res. 48 (2009) 373–379, https://doi.org/10.1021/ie800870k.
[79] S.K. Hoekman, A. Broch, C. Robbins, Hydrothermal carbonization (HTC) of lignocellulosic biomass, Energy Fuels 25 (2011) 1802–1810, https://doi.org/10.1021/ef101745n.
[80] J.G. Lynam, C.J. Coronella, W. Yan, M.T. Reza, V.R. Vasquez, Acetic acid and lithium chloride effects on hydrothermal carbonization of lignocellulosic biomass, Bioresour. Technol. 102 (2011) 6192–6199, https://doi.org/10.1016/j.biortech.2011.02.035.
[81] W. Yan, T.C. Acharjee, C.J. Coronella, V.R. Vásquez, Thermal pretreatment of lignocellulosic biomass, Environ. Prog. Sustain. Energy 28 (2009) 435–440, https://doi.org/10.1002/ep.10385.
[82] W. Zhao, L. Luo, H. Wang, M. Fan, Synthesis of bamboo-based activated carbons with super-high specific surface area for hydrogen storage, BioResources 12 (2017) 1246–1262, https://doi.org/10.15376/biores.12.1.1246-1262.
[83] J.H. Hassen, Effect of KOH ratio on the formation of activated carbon from pressed wood residues, Int. J. Pharm. Sci. Res. 8 (2017) 4875–4880.
[84] R.K. Liew, E. Azwar, P.N.Y. Yek, X.Y. Lim, C.K. Cheng, J.-H. Ng, A. Jusoh, W. H. Lam, M.D. Ibrahim, N.L. Ma, S.S. Lam, Microwave pyrolysis with KOH/NaOH mixture activation: a new approach to produce micro-mesoporous activated carbon for textile dye adsorption, Bioresour. Technol. 266 (2018) 1–10, https://doi.org/10.1016/j.biortech.2018.06.051.
[85] S.A. Opatokun, A. Prabhu, A. Al Shoaibi, C. Srinivasakannan, V. Strezov, Food wastes derived adsorbents for carbon dioxide and benzene gas sorption, Chemosphere 168 (2017) 326–332, https://doi.org/10.1016/j.chemosphere.2016.10.083.
[86] M. Han, K. Jiang, P. Jiao, Y. Ji, J. Zhou, W. Zhuang, Y. Chen, D. Liu, C. Zhu, X. Chen, H. Ying, J. Wu, Bio-butanol sorption performance on novel porous-carbon adsorbents from corncob prepared via hydrothermal carbonization and post-pyrolysis method, Sci. Rep. 7 (2017), https://doi.org/10.1038/s41598-017-12062-7.
[87] A.-N.A. El-Hendawy, An insight into the KOH activation mechanism through the production of microporous activated carbon for the removal of Pb2+ cations, Appl. Surf. Sci. 255 (2009) 3723–3730, https://doi.org/10.1016/j.apsusc.2008.10.034.
[88] M.A. Lillo-Ródenas, D. Cazorla-Amorós, A. Linares-Solano, Understanding chemical reactions between carbons and NaOH and KOH: an insight into the chemical activation mechanism, Carbon 41 (2003) 267–275, https://doi.org/10.1016/S0008-6223(02)00279-8.
[89] S. Jun, S.H. Joo, R. Ryoo, M. Kruk, M. Jaroniec, Z. Liu, T. Ohsuna, O. Terasaki, Synthesis of new, nanoporous carbon with hexagonally ordered mesostructure, J. Am. Chem. Soc. 122 (2000) 10712–10713, https://doi.org/10.1021/ja002261e.
[90] M.S. Balathanigaimani, Md.B. Haider, D. Jha, R. Kumar, S.J. Lee, W.G. Shim, H. K. Shon, S.C. Kim, H. Moon, Nanostructured Biomass Based Carbon Materials from Beer Lees for Hydrogen Storage, J. Nanosci. Nanotechnol. 18 (2018) 2196–2199, https://doi.org/10.1166/jnn.2018.15001.
[91] F. Schüth, K.S.W. Sing, J. Weitkamp, Handbook of Porous Solids, Wiley-Vch, 2002.
[92] M. Thommes, K. Kaneko, A.V. Neimark, J.P. Olivier, F. Rodriguez-Reinoso, J. Rouquerol, K.S. Sing, Physisorption of gases, with special reference to the evaluation of surface area and pore size distribution (IUPAC Technical Report), Pure Appl. Chem. 87 (2015) 1051–1069.
[93] W. Zhao, M. Fan, H. Gao, H. Wang, Central composite design approach towards optimization of super activated carbons from bamboo for hydrogen storage, RSC Adv. 6 (2016) 46977–46983, https://doi.org/10.1039/C6RA06326H.
[94] Z. Zheng, Q. Gao, J. Jiang, High hydrogen uptake capacity of mesoporous nitrogen-doped carbons activated using potassium hydroxide, Carbon 48 (2010) 2968–2973, https://doi.org/10.1016/j.carbon.2010.04.037.
[95] R. Yang, G. Liu, M. Li, J. Zhang, X. Hao, Preparation and N2, CO2 and H2 adsorption of super activated carbon derived from biomass source hemp (Cannabis sativa L.) stem, Microporous Mesoporous Mater. 158 (2012) 108–116, https://doi.org/10.1016/j.micromeso.2012.03.004.
[96] T. Chen, Y. Zhou, L. Luo, X. Wu, Z. Li, M. Fan, W. Zhao, Preparation and characterization of heteroatom self-doped activated biocarbons as hydrogen storage and supercapacitor electrode materials, Electrochim. Acta 325 (2019) 134941, https://doi.org/10.1016/j.electacta.2019.134941.
[97] L. Wang, Y. Guo, B. Zou, C. Rong, X. Ma, Y. Qu, Y. Li, Z. Wang, High surface area porous carbons prepared from hydrochars by phosphoric acid activation, Bioresour. Technol. 102 (2011) 1947–1950.
[98] H.B. Sharma, B.K. Dubey, Co-hydrothermal carbonization of food waste with yard waste for solid biofuel production: hydrochar characterization and its pelletization, Waste Manag. 118 (2020) 521–533, https://doi.org/10.1016/j.wasman.2020.09.009.
[99] N.U. Saqib, S. Baroutian, A.K. Sarmah, Physicochemical, structural and combustion characterization of food waste hydrochar obtained by hydrothermal carbonization, Bioresour. Technol. 266 (2018) 357–363, https://doi.org/10.1016/j.biortech.2018.06.112.
[100] H. Sun, A. Li, Z. Zhu, W. Liang, X. Zhao, P. La, W. Deng, Superhydrophobic activated carbon-coated sponges for separation and absorption, Chem. Sus. Chem. 6 (2013) 1057–1062.
[101] F. Sun, L. Wang, Y. Peng, J. Gao, X. Pi, Z. Qu, G. Zhao, Y. Qin, Converting biomass waste into microporous carbon with simultaneously high surface area and carbon purity as advanced electrochemical energy storage materials, Appl. Surf. Sci. 436 (2018) 486–494, https://doi.org/10.1016/j.apsusc.2017.12.067.
[102] T. Ramesh, N. Rajalakshmi, K.S. Dhathathreyan, Synthesis and characterization of activated carbon from jute fibers for hydrogen storage, Renew. Energy Environ. Sustain. 2 (2017) 4, https://doi.org/10.1051/rees/2017001.
[103] F. Ding, B.I. Yakobson, Challenges in hydrogen adsorptions: from physisorption to chemisorption, Front. Phys. 6 (2011) 142–150, https://doi.org/10.1007/s11467-011-0171-6.
[104] R.K. Agarwal, J.S. Noh, J.A. Schwarz, P. Davini, Effect of surface acidity of activated carbon on hydrogen storage, Carbon 25 (1987) 219–226, https://doi.org/10.1016/0008-6223(87)90119-9.
[105] DOE Technical Targets for Onboard Hydrogen Storage for Light-Duty Vehicles, Energy.Gov. (n.d.). https://www.energy.gov/eere/fuelcells/doe-technical-targets-onboard-hydrogen-storage-light-duty-vehicles (accessed August 1, 2021).